Fermionic electroweak NNLO corrections to $e^+e^- \rightarrow ZH$ with polarized beams and different renormalization schemes

Ayres Freitas,* Qian Songo,† and Keping Xie[‡]

Pittsburgh Particle-physics Astro-physics and Cosmology Center (PITT-PACC),

Department of Physics and Astronomy, University of Pittsburgh,

Pittsburgh, Pennsylvania 15260, USA

(Received 16 June 2023; accepted 2 September 2023; published 18 September 2023)

Recently, the next-to-next-to-leading order (NNLO) electroweak corrections with fermion loops to the Higgsstrahling process were computed. Here we present numerical results for polarized electron/positron beams, as well as for two input parameter schemes known as the $\alpha(0)$ and G_{μ} schemes. The size of the NNLO corrections strongly depends on the beam polarization, leading to an increase of the ZH cross section by 0.76% for $e_L^+e_R^-$ beams, and a decrease of 0.04% for $e_R^+e_L^-$ beams. Furthermore, inclusion of the NNLO corrections is found to significantly reduce the discrepancy between the results in the $\alpha(0)$ and G_{μ} schemes. Using the remaining difference, together with other methods, the theory uncertainty from missing bosonic electroweak corrections is estimated to be less than 0.3%.

DOI: 10.1103/PhysRevD.108.053006

I. INTRODUCTION

A high-luminosity e^+e^- collider operating at center-of-mass energies of 240–250 GeV can perform model-independent precision measurements of the properties of the recently discovered Higgs boson. Several collider concepts have been proposed for this purpose; the International Linear Collider (ILC) [1,2], the Future Circular Collider (FCC-ee) [3], and the Circular Electron-Positron Collider (CEPC) [4]. The cross section for the main production process, $e^+e^- \rightarrow ZH$, is projected to be measured with percent level precision at these facilities (1.2% at ILC, 0.4% at FCC-ee, and 0.5% at CEPC). Any deviations from the Standard Model (SM) expectation can be interpreted as sign of new physics beyond the SM.

Such an interpretation requires sufficiently accurate theoretical predictions for *ZH* production within the SM, including higher-order radiative corrections. While the next-to-leading order (NLO) corrections have been known since many years [5–7], the mixed electroweak-QCD next-to-next-to-leading order (NNLO) corrections have been computed more recently [8,9]. Very recently, the fermionic electroweak NNLO corrections have been completed [10],

Published by the American Physical Society under the terms of the Creative Commons Attribution 4.0 International license. Further distribution of this work must maintain attribution to the author(s) and the published article's title, journal citation, and DOI. Funded by SCOAP³. where "fermionic" denotes contributions from diagrams with closed fermion loops. There is also ongoing work to compute the full electroweak NNLO corrections, including "bosonic" contributions [11].

This article expands on the work of Ref. [10] by including the effect of beam polarization and different renormalization schemes. Beam polarization can help to disentangle the nature of potential new physics effects in ZH production. The SM NLO corrections to $e^+e^- \rightarrow ZH$ with polarized beams have been presented in Ref. [12]. Here, this is extended by also computing the fermionic electroweak NNLO corrections.

In addition, we present NNLO results for two different renormalization schemes. One scheme, called the $\alpha(0)$ scheme, uses the electromagnetic coupling, together with particle masses, as inputs to specify the SM parameters. This scheme has been used in Ref. [10]. Alternatively, the G_{μ} scheme instead uses the Fermi constant as an input to define the electromagnetic coupling strength. The numerical difference between the predictions in the two schemes can be taken as a proxy for the impact of missing higher-order corrections.

II. POLARIZED CROSS SECTIONS

The perturbative expansion of the squared matrix element \mathcal{M} takes the following form:

$$\begin{split} |\mathcal{M}|^2 &= |\mathcal{M}_{(0)}|^2 \quad \text{(LO)} \\ &+ 2 \text{Re} \{\mathcal{M}_{(0)}^* \mathcal{M}_{(1)}\} \quad \text{(NLO)} \\ &+ |\mathcal{M}_{(1)}|^2 + 2 \text{Re} \{\mathcal{M}_{(0)}^* \mathcal{M}_{(2)}\} \quad \text{(NNLO)}, \end{split} \tag{1}$$

^{*}afreitas@pitt.edu

[†]qis26@pitt.edu

[‡]xiekeping@pitt.edu

where the subscript indicates the loop order. For the process $e^+e^- \rightarrow ZH$, the matrix element has the form

$$\mathcal{M}_{(n)} = \bar{v}(p_{e^+}) \Gamma^{\mu}_{(n)} u(p_{e^-}) \varepsilon_{\mu}, \qquad (2)$$

where $p_{e^{\pm}}$ are the momenta of the incoming electron and positron, respectively, and ε_{μ} is the polarization vector of the outgoing Z boson. For the unpolarized cross section, one needs to average of initial spins, which is accomplished by the Carsimir trace technique,

$$\frac{1}{4} \sum_{e^{\pm} \text{spins}} \mathcal{M}_{(m)}^* \mathcal{M}_{(n)} = \frac{1}{4} \text{Tr} \Big\{ \bar{\Gamma}_{(m)}^{\mu} \not\!\!{p}_{e^{+}} \Gamma_{\mu,(n)} \not\!\!{p}_{e^{-}} \Big\}, \quad (3)$$

where the electron mass has been neglected.

On the other hand, the results for left-/right-handed polarized electron and positron beams are obtained by inserting polarization projectors $P_{\rm R,L} = (1 \pm \gamma^5)/2$,

$$\mathcal{M}_{(m)}^{*} \mathcal{M}_{(n)} \Big|_{e_{j}^{+} e_{k}^{-}} = \frac{1}{4} \operatorname{Tr} \Big\{ \bar{\Gamma}_{(m)}^{\mu} \not\!\!{p}_{e^{+}} P_{j} \Gamma_{\mu,(n)} P_{k} \not\!\!{p}_{e^{-}} \Big\}$$

$$(j, k = L, R), \tag{4}$$

After this step, the remaining calculation proceeds just in the same way as for the unpolarized cross section. In particular, the nontrivial two-loop integrals can be computed with the techniques described in Refs. [10,13]. One of the of the two subloops simplified using Feynman parameters and then expressed in terms of an dispersion integral. This allows one to solve the second subloop integral analytically in terms of well-known one-loop Passarino-Veltman functions. Ultraviolet divergencies are removed with suitable subtraction terms, which can be integrated analytically and then added back. Additional technical aspects of the computation of the subtraction terms are given in the Appendix. Finally, the finite remainder integral is integrated numerically over the Feynman parameters and the dispersion variable. See Refs. [10,13] for more details.

Instead of separately going through all the steps of the computation for left- and right-handed polarized beams, one can alternatively derive the polarized matrix elements from the unpolarized one, which seems more efficient for calculating the two-loop diagrams. This is achieved by grouping certain types of diagrams. Considering a two-loop diagram where the incoming fermion line connects with N gauge bosons (γ or Z), the polarized matrix elements satisfy the relationships

$$\begin{split} M_{(2)}^{V_1\cdots V_N*}M_{(0)}\Big|_{e_R^+e_L^-} &= \frac{4g_L^{eeZ}g_L^{eeV_1}\cdots g_L^{eeV_N}}{g_L^{eeZ}g_L^{eeV_1}\cdots g_L^{eeV_N}+g_R^{eeZ}g_R^{eeV_1}\cdots g_R^{eeV_N}} \\ & \times \left[M_{(2)}^{V_1\cdots V_N*}M_{(0)}\right]_{\mathrm{unpol}}, \\ M_{(2)}^{V_1\cdots V_N*}M_{(0)}\Big|_{e_L^+e_R^-} &= \frac{4g_R^{eeZ}g_R^{eeV_1}\cdots g_R^{eeV_N}}{g_L^{eeZ}g_L^{eeV_1}\cdots g_L^{eeV_N}+g_R^{eeZ}g_R^{eeV_1}\cdots g_R^{eeV_N}} \\ & \times \left[M_{(2)}^{V_1\cdots V_N*}M_{(0)}\right]_{\mathrm{unpol}}, \\ M_{(2)}^{V_1\cdots V_N*}M_{(0)}\Big|_{e_L^+e_L^-} &= M_{(2)}^{V_1\cdots V_N*}M_{(0)}\Big|_{e_R^+e_R^-} &= 0, \end{split}$$

where $g_{L(R)}^{eeV}$ is the left(right)-handed coupling of eeV vertex

If the fermion line connects only with W bosons, which only interact with left-handed fermions, thus we end up with very simple equations

$$M_{(2)}^{W_1 \cdots W_N *} M_{(0)} \Big|_{e_R^+ e_L^-} = 4 \Big[M_{(2)}^{W_1 \cdots W_N *} M_{(0)} \Big]_{\text{unpol}},$$

$$M_{(2)}^{W_1 \cdots W_N *} M_{(0)} \Big|_{e_I^+ e_R^-} = 0.$$
(6)

Numerical results for the polarized cross section are presented in Table I, using the following input parameters:

$$m_W^{\text{exp}} = 80.379 \text{ GeV} \Rightarrow m_W = 80.352 \text{ GeV},$$
 $m_Z^{\text{exp}} = 91.1876 \text{ GeV} \Rightarrow m_Z = 91.1535 \text{ GeV},$
 $m_H = 125.1 \text{ GeV}, \qquad m_t = 172.76 \text{ GeV},$
 $\alpha^{-1} = 137.036, \qquad \Delta\alpha = 0.059,$
 $\sqrt{s} = 240 \text{ GeV},$
(7)

where \sqrt{s} represents the center-of-mass energy, and the masses of all the other fermions are set to be 0. Furthermore, $\Delta \alpha = 1 - \alpha (m_Z)/\alpha(0)$ accounts for the running of the electromagnetic coupling between the

TABLE I. Numerical results for the integrated ZH production cross section, in fb, at LO, NLO, and fermionic electroweak NNLO, for different beam polarizations. The results are for the $\alpha(0)$ renormalization scheme and $\sqrt{s}=240$ GeV. The electroweak NNLO corrections are also listed individually according to the number of fermion loops symbolized as N_f .

	$e^+_{ m R} e^{ m L}$	$e_{ m L}^+e_{ m R}^-$
σ^{LO} [fb]	541.28	350.55
$\sigma^{\rm NLO}$ [fb]	507.92	411.66
σ^{NNLO} [fb]	507.51	418.68
$\mathcal{O}(lpha_{N_f=2}^2)$	1.75	5.77
$\mathcal{O}(lpha_{N_f=1}^2)$	-2.15	1.25

Thomson limit and the weak scale, and it includes nonperturbative hadronic effects.

Since the Z and W bosons have sizeable decay widths, their masses (m_Z and m_W) are defined via the complex pole of the gauge-boson propagators. This definition is theoretically well-defined but it differs from the one that is commonly used in experimental studies. The relation between the two is given by [14]

$$m_Z = m_Z^{\text{exp}} [1 + (\Gamma_Z^{\text{exp}}/m_Z^{\text{exp}})^2]^{-1/2},$$
 (8)

$$\Gamma_Z = \Gamma_Z^{\text{exp}} [1 + (\Gamma_Z^{\text{exp}}/m_Z^{\text{exp}})^2]^{-1/2}.$$
 (9)

The numerical results presented in this paper do not include QED initial-state radiation (ISR). At the order that we are working, QED ISR factorizes and can be taken into account through convolution with a universal structure function.¹

As can be seen from Table I, the electroweak NNLO corrections depend strongly on the beam polarization. The contributions with two closed fermion loops $(N_f=2)$ are significantly larger for right-handed electron polarization and left-handed positron polarization than for the opposite case. The contribution with one closed fermion loop $(N_f=1)$ has opposite signs for the two polarization, which leads to an accidental cancellation for the unpolarized cross section.

The higher-order corrections also modify the shape of the differential cross section, and the specific form of this modification depends on the beam polarization. This is illustrated in Fig. 1, which shows the cross section as a function of the scattering angle θ at different orders of perturbation theory for two beam polarizations. As can be seen from the figure, the shape distortions from the NNLO corrections are not very large, but non-negligible.

III. RESULTS FOR DIFFERENT RENORMALIZATION SCHEMES

The on-shell (OS) renormalization scheme defines the masses of all elementary particles via the (complex) propagator pole. In our calculation, this prescription is applied to the gauge boson masses, $m_{Z,W}$, the Higgs boson mass, m_H , and the top-quark mass, m_t . All other fermion masses are neglected. As already mentioned in the previous section, the finite width of the Z and W bosons needs to be taken into account, so that the poles of their propagators become complex. In deriving the Z/W mass counterterms, the power counting $\Gamma_{Z,W}/m_{Z,W} \sim \mathcal{O}(\alpha)$ is used, i.e., one performs a simultaneous expansion in the coupling constant and the gauge-boson widths. Since the Higgs-boson width is very small and the top quark only appear inside of

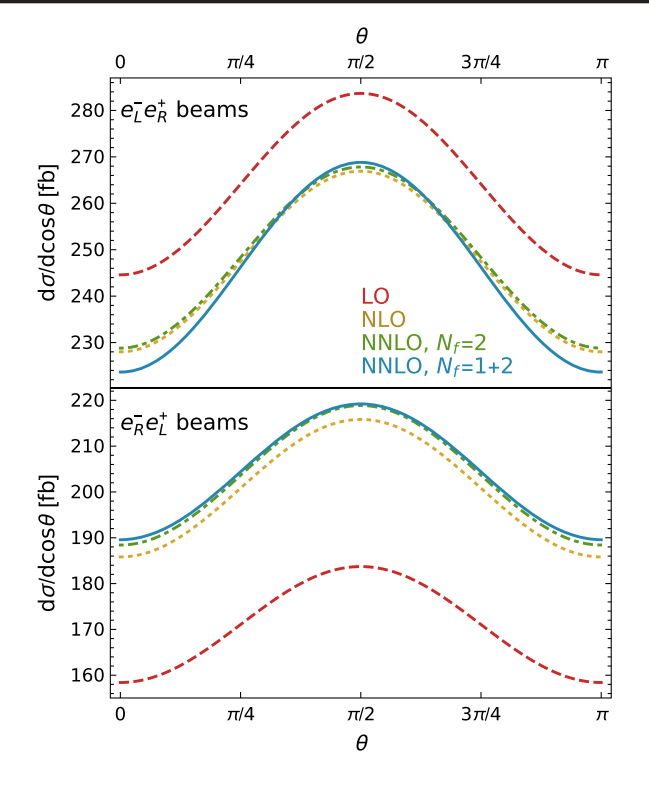


FIG. 1. Differential cross sections, as a function of the scattering angle θ , for two different beam polarizations. As in Table I, the plots are based on the $\alpha(0)$ renormalization scheme and $\sqrt{s}=240$ GeV.

loop contributions, their widths can be neglected. More details on the mass renormalization can be found, e.g., in Ref. [15].

In addition, one needs a renormalization prescription for the electroweak coupling strength. In the following, two different schemes for this purpose are compared. One scheme, called the $\alpha(0)$ scheme, defines $\alpha=e^2/(4\pi)$ as the electromagnetic coupling at zero momentum, and the weak coupling is defined via

$$g = \frac{e}{\sin \theta_W} = \frac{e}{\sqrt{1 - m_W^2 / m_Z^2}}$$
 (10)

to all orders in perturbation theory. This scheme is sensitive to the running of $\alpha(Q)$ from Q=0 to the weak scale, and it needs $\Delta \alpha$ as a numerical input.

The second scheme, called the G_{μ} scheme, relates the weak coupling to the Fermi coupling G_{μ} ,

$$\frac{G_{\mu}}{\sqrt{2}} = \frac{g^2}{8m_W^2} (1 + \Delta r). \tag{11}$$

The numerical value for G_{μ} is extracted from the measured muon lifetime [16]. The quantity Δr contains radiative corrections that are determined by matching the muon decay matrix element in the Fermi theory and the full SM.

¹For the bosonic NNLO corrections, which have not been computed in this work, the infrared divergencies from ISR would still factorize, but there would be a finite remainder from some mixed OED-weak diagrams.

TABLE II. Numerical results for the unpolarized integrated ZH production cross section, in fb, for two different renormalization schemes. Results are given for $\sqrt{s} = 240$ GeV at LO, NLO, and fermionic electroweak NNLO. For the latter, the contributions from two $(N_f = 2)$ and one $(N_f = 1)$ closed fermion loops are also shown individually.

	$\alpha(0)$ scheme	G_{μ} scheme
σ^{LO} [fb]	222.96	239.18
$\sigma^{\rm NLO}$ [fb]	229.89	232.08
$\sigma^{\rm NNLO}$ [fb]	231.55	232.74
$\mathcal{O}(lpha_{N_f=2}^2)$	1.88	0.73
$\mathcal{O}(\alpha_{N_f=1}^2)$	-0.23	-0.07

We use NLO and fermionic NNLO results for Δr from Refs. [15,17] (also see Ref. [18]). The electromagnetic coupling in the G_{μ} scheme is derived from g by again using Eq. (10). Note that this scheme does not depend on the shift $\Delta \alpha$ of the running electromagnetic coupling.

Using the input parameters in Eq. (7), together with $G_{\mu} = 1.1663787 \times 10^{-5}$, the results obtained in the two renormalization schemes are shown in Table II. As can be seen from the table, the numerical agreement between the results in the two schemes improves with each order in perturbation theory, as expected.

In fact, this convergence is further improved when including the mixed electroweak-QCD two-loop corrections [8,9]. We use numerical results for this contribution from Ref. [9]. In order to do so, we have to compute our electroweak corrections for the same input parameters used there. The results are shown in Table III.

The prediction for the cross section including all available results agrees very well between the two renormalization schemes, with a difference of 0.12 fb. This difference is due to missing higher-order corrections, where the dominant impact is expected from the bosonic electroweak NNLO corrections, i.e., from two-loop contributions without closed fermion loops.

Therefore, one can use the difference between the two renormalization schemes as an order-of-magnitude estimate of the perturbative theory uncertainty. Since this estimate is only a lower bound on the size of missing higher-order contributions, we conservatively multiply it by a factor 2, to arrive at an error estimate of 0.24 fb.

TABLE III. Similar to Table II, but using input values and mixed EW-QCD corrections from Ref. [9].

	$\alpha(0)$ scheme	G_{μ} scheme
$\sigma^{\rm LO}$ [fb]	223.14	239.64
$\sigma^{\rm NLO}$ [fb]	229.78	232.46
$\sigma^{\text{NNLO,EW} \times \text{QCD}}$ [fb]	232.21	233.29
$\sigma^{\mathrm{NNLO,EW}}$ [fb]	233.86	233.98

An alternative estimate of the bosonic NNLO corrections could be obtained by considering a subset of the latter; namely, those stemming from $|\mathcal{M}_{(1,bos)}|^2$, where $\mathcal{M}_{(1,bos)}$ is the matrix element of the bosonic NLO corrections. This leads to a contribution of 0.65 fb to the cross section. The contribution from genuine bosonic two-loop diagrams, $2\text{Re}\{\mathcal{M}^*_{(0)}\mathcal{M}_{(2,bos)}\}$, is expected to be smaller than this, since the Born matrix element $\mathcal{M}_{(0)}$ contains several suppression factors: (a) the e-e-Z couplings in the initial state are smaller than the $e-\nu-W$ couplings, which appear in the 1-loop box diagrams, by a factor $2^{-3/2} \sim 0.35$; (b) the *s*-channel *Z* propagator produces a factor $m_Z^2/(s-m_Z^2) \sim 0.17$ for $\sqrt{s}=240$ GeV.

Thus, it seems plausible that the missing bosonic electroweak NNLO corrections have an impact between 0.24 fb and 0.65 fb on the SM prediction for the ZH production cross section. These theory error estimates are lower than the anticipated experimental precision (0.4-1%), but a direct calculation of these missing contributions is still desirable.

IV. CONCLUSIONS

In this article, we present the calculation of the $e^+e^- \rightarrow$ ZH cross section with polarized beams, while also addressing the renormalization scheme dependence. The electroweak NNLO corrections exhibit a strong dependence on the beam polarizations. The corrections are found to be large for $e_L^+e_R^-$ beam polarization, while small for $e_R^+e_L^-$ case due to numerical cancellation. By computing the cross section in the $\alpha(0)$ and G_u schemes, we have shown that the renormalization scheme dependence decreases by including the two-loop electroweak corrections, and reduces further by adding mixed EW-QCD corrections. Renormalization scheme dependence can be utilized to estimate missing higher order corrections. Combining this with partial results for the missing bosonic electroweak NNLO corrections, we estimate the latter to be about 0.1–0.3%, thus lower than the anticipated experimental precision (0.4–1%).

ACKNOWLEDGMENTS

This work has been supported in part by the National Science Foundation under Grant No. PHY-2112829.

APPENDIX: UV SUBTRACTION TERMS

The UV divergent subtraction terms must be expanded appropriately to get the correct finite term. As stated in Ref. [10], there are three types of subtraction terms; two for subloop divergences and one more for a global divergence. The latter corresponds to vacuum diagrams, the analytical formulas of which can be obtained and expanded to higher orders in ϵ with TVID [19]. The general form for the subloop divergences can be expressed as the multiplication of two one-loop scalar integrals. Taking the two-loop vertex

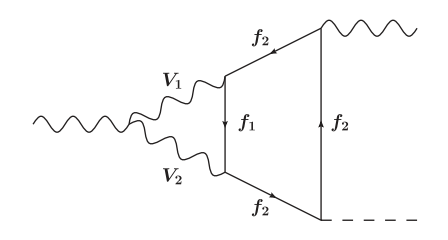


FIG. 2. Two-loop VZH vertex diagram.

diagram Fig. 2 as an example, the tensor integral can be written as

$$I = \int \frac{d^{D}q_{2}}{i\pi^{2}} \frac{d^{D}q_{1}}{i\pi^{2}} \sum_{n_{0},n_{1},n_{2},i,j} c_{ij}^{n_{0},n_{1},n_{2}} \times \left\{ p_{i}^{n_{0}}, q_{1}^{n_{1}}, q_{2}^{n_{2}} \right\}_{j}$$

$$\times \frac{1}{(q_{2}^{2} - m_{V_{2}}^{2})((q_{2} + p)^{2} - m_{V_{1}}^{2})((q_{2} + q_{1})^{2} - m_{f_{1}}^{2})}$$

$$\times \frac{1}{(q_{1}^{2} - m_{f_{2}}^{2})((q_{1} - p_{h})^{2} - m_{f_{2}}^{2})((q_{1} - p)^{2} - m_{f_{2}}^{2})},$$
(A1)

where $\{p_i^{n_0}, q_1^{n_1}, q_2^{n_2}\}$ denotes dot products among external momentum p_i and loop momentum $q_{1,2}$, and n_i denote the power of each of them. The index j labels all possible dot product conditions. For example for $n_0 = 0$, $n_1 = n_2 = 2$, the possible dot products read

$$\{p_i^0, q_1^2, q_2^2\}_1 = (q_1 \cdot q_1)(q_2 \cdot q_2),$$

$$\{p_i^0, q_1^2, q_2^2\}_2 = (q_1 \cdot q_2)(q_1 \cdot q_2).$$
 (A2)

The SM Feynman rules require that $n_1 \le 4$, $n_2 \le 2$, $n_0 + n_1 + n_2 \le 6$. $c_{ij}^{n_0,n_1,n_2}$ is the coefficient of a dot product, and it is a function of masses and dimension D. The integral (A1) contains a subloop divergence from the q_1 loop, which originate from the numerators $q_1^{n_1}$ with $n_1 \ge 4$. To make the q_1 integral UV finite, the following subtraction term is constructed:

$$I_{\text{subtr}}^{q_{1}} = \int \frac{d^{D}q_{2}}{i\pi^{2}} \frac{d^{D}q_{1}}{i\pi^{2}} \sum_{i,j} \left[c_{ij}^{2,4,0} \times \{p_{i}^{2}, q_{1}^{4}, q_{2}^{0}\}_{j} + c_{ij}^{1,4,1} \times \{p_{i}^{1}, q_{1}^{4}, q_{2}^{1}\}_{j} + c_{ij}^{0,4,2} \times \{p_{i}^{0}, q_{1}^{4}, q_{2}^{2}\}_{j} \right]$$

$$+ c_{ij}^{1,4,0} \times \{p_{i}^{1}, q_{1}^{4}, q_{2}^{0}\}_{j} + c_{ij}^{0,4,1} \times \{p_{i}^{0}, q_{1}^{4}, q_{2}^{1}\}_{j} + c_{ij}^{0,4,0} \times \{p_{i}^{0}, q_{1}^{4}, q_{2}^{0}\}_{j}$$

$$\times \frac{1}{(q_{2}^{2} - m_{V_{2}}^{2})((q_{2} + p)^{2} - m_{V_{1}}^{2})(q_{1}^{2} - m_{f_{1}}^{2})} \frac{1}{(q_{1}^{2} - m_{f_{2}}^{2})(q_{1}^{2} - m_{f_{2}}^{2})(q_{1}^{2} - m_{f_{2}}^{2})}.$$
(A3)

From Eq. (A3), one can see that the loop integrals of q_1 and q_2 are disentangled. After performing the loop integration, one obtains

$$I_{\text{subtr}}^{q_1} = B_0(p^2, m_{V_2}^2, m_{V_1}^2) \times \left[a_1 A_0(m_{f_1}^2) + a_2 A_0(m_{f_2}^2) \right], \tag{A4}$$

where a_i are functions of masses, external momenta and dimension D. A similar subloop subtraction term needs to be introduced in the vacuum integrals for the global divergence. Combining the two subloop subtraction terms, we obtain

$$\begin{split} I_{\text{subtr}} &= \left[B_0(p^2, m_{V_2}^2, m_{V_1}^2) - B_0(0, m_{V_2}^2, m_{V_1}^2)\right] \\ &\times \left[a_1 A_0(m_{f_1}^2) + a_2 A_0(m_{f_2}^2)\right]. \end{split} \tag{A5}$$

This term can now be expanded in powers of $\epsilon = (4 - D)/2$, resulting in the expressions

$$I_{\text{subtr}}^{\text{div}} = \left[B_0^{(0)}(p^2, m_{V_2}^2, m_{V_1}^2) - B_0^{(0)}(0, m_{V_2}^2, m_{V_1}^2) \right] \times \left[a_1^{(0)} A_0^{(-1)}(m_{f_1}^2) + a_2^{(0)} A_0^{(-1)}(m_{f_2}^2) \right], \tag{A6}$$

$$\begin{split} I_{\text{subtr}}^{\text{fin}} &= \left[B_0^{(0)}(p^2, m_{V_2}^2, m_{V_1}^2) - B_0^{(0)}(0, m_{V_2}^2, m_{V_1}^2) \right] \\ &\times \left[a_1^{(0)} A_0^{(0)}(m_{f_1}^2) + a_2^{(0)} A_0^{(0)}(m_{f_2}^2) \right. \\ &+ a_1^{(1)} A_0^{(-1)}(m_{f_1}^2) + a_2^{(1)} A_0^{(-1)}(m_{f_2}^2) \right] \\ &+ \left[B_0^{(1)}(p^2, m_{V_2}^2, m_{V_1}^2) - B_0^{(1)}(0, m_{V_2}^2, m_{V_1}^2) \right] \\ &\times \left[a_1^{(0)} A_0^{(-1)}(m_{f_1}^2) + a_2^{(0)} A_0^{(-1)}(m_{f_2}^2) \right], \end{split} \tag{A7}$$

where (n) denote the expansion order in ϵ . Eq. (A7) indicates that $\mathcal{O}(\epsilon)$ parts of one-loop scalar functions must be taken into account. Analytical expressions for these can be found in Ref. [20].

- [1] H. Baer *et al.*, The international linear collider technical design report—Volume 2: Physics, arXiv:1306.6352.
- [2] P. Bambade *et al.*, The international linear collider: A global project, arXiv:1903.01629.
- [3] A. Abada *et al.* (FCC Collaboration), FCC-ee: The lepton collider: Future circular collider conceptual design report Volume 2, Eur. Phys. J. Special Topics 228, 261 (2019).
- [4] J. B. Guimarães da Costa et al. (CEPC Study Group), CEPC conceptual design report: Volume 2—Physics & detector, arXiv:1811.10545.
- [5] J. Fleischer and F. Jegerlehner, Radiative corrections to Higgs production by $e^+e^- \rightarrow ZH$ in the {Weinberg-Salam} model, Nucl. Phys. **B216**, 469 (1983).
- [6] B. A. Kniehl, Radiative corrections for associated ZH production at future e^+e^- colliders, Z. Phys. C **55**, 605 (1992).
- [7] A. Denner, J. Küblbeck, R. Mertig, and M. Böhm, Electroweak radiative corrections to $e^+e^- \rightarrow ZH$, Z. Phys. C **56**, 261 (1992).
- [8] Y. Gong, Z. Li, X. Xu, L. L. Yang, and X. Zhao, Mixed QCD-EW corrections for Higgs boson production at e^+e^- colliders, Phys. Rev. D **95**, 093003 (2017).
- [9] Q. F. Sun, F. Feng, Y. Jia, and W. L. Sang, Mixed electroweak-QCD corrections to e + e− → HZ at Higgs factories, Phys. Rev. D 96, 051301(R) (2017).
- [10] A. Freitas and Q. Song, Two-Loop Electroweak Corrections with Fermion Loops to $e + e \rightarrow ZH$, Phys. Rev. Lett. **130**, 031801 (2023).
- [11] X. Chen, X. Guan, C. Q. He, Z. Li, X. Liu, and Y. Q. Ma, Complete two-loop electroweak corrections to $e^+e^- \rightarrow HZ$, arXiv:2209.14953.

- [12] S. Bondarenko, Y. Dydyshka, L. Kalinovskaya, L. Rumyantsev, R. Sadykov, and V. Yermolchyk, One-loop electroweak radiative corrections to polarized $e^+e^- \rightarrow ZH$, Phys. Rev. D **100**, 073002 (2019).
- [13] Q. Song and A. Freitas, On the evaluation of two-loop electroweak box diagrams for $e^+e^- \rightarrow HZ$ production, J. High Energy Phys. 04 (2021) 179.
- [14] D. Y. Bardin, A. Leike, T. Riemann, and M. Sachwitz, Energy dependent width effects in e + e- annihilation near the Z boson pole, Phys. Lett. B **206**, 539 (1988).
- [15] A. Freitas, W. Hollik, W. Walter, and G. Weiglein, Electroweak two loop corrections to the $M_W M_Z$ mass correlation in the standard model, Nucl. Phys. **B632**, 189 (2002); **B666**, 305(E) (2003). [arXiv:hep-ph/0202131].
- [16] R. L. Workman *et al.* (Particle Data Group), Review of particle physics, Prog. Theor. Exp. Phys. **2022**, 083C01 (2022).
- [17] A. Freitas, W. Hollik, W. Walter, and G. Weiglein, Complete fermionic two loop results for the M_W – M_Z interdependence, Phys. Lett. B **495**, 338 (2000); **570**, 265(E) (2003).
- [18] M. Awramik and M. Czakon, Complete two loop electroweak contributions to the muon lifetime in the standard model, Phys. Lett. B 568, 48 (2003).
- [19] S. Bauberger, A. Freitas, and D. Wiegand, TVID 2: Evaluation of planar-type three-loop self-energy integrals with arbitrary masses, J. High Energy Phys. 01 (2020) 024.
- [20] U. Nierste, D. Muller, and M. Bohm, Two loop relevant parts of D-dimensional massive scalar one loop integrals, Z. Phys. C 57, 605 (1993).